One-dimensional structured ultrasonic metamaterials with simultaneously negative dynamic density and modulus

Y. Cheng, J. Y. Xu, and X. J. Liu*
Key Lab of Modern Acoustics, Nanjing University, Nanjing 210093, China
(Received 26 March 2007; revised manuscript received 18 August 2007; published 29 January 2008)

We present theoretically a type of one-dimensional (1D) structured ultrasonic metamaterial that exhibits a forbidden band where both the effective dynamic density and bulk modulus are simultaneously negative. The material consists of a 1D array of repeated unit cells with shunted Helmholtz resonators. The transmission coefficient, wave vector, negative dynamic density, and modulus are determined by means of the acoustic transmission line method (ATLM). The double negativity in the effective dynamic density and bulk modulus is an acoustic counterpart of negative permittivity and permeability in the electromagnetic metamaterials. The double negative band is ascribed to the local resonance. In order to confirm the ATLM results, we further calculate the field intensity, phase distribution, and transmission coefficient using the finite element method. In addition, the influences of some essential geometric acoustic parameters on the transmission properties, such as periodic constant L, are also discussed.

DOI: 10.1103/PhysRevB.77.045134 PACS number(s): 43.35.+d, 43.20.+g, 46.40.Cd

I. INTRODUCTION

Left-handed material was proposed as a theoretical possibility.[1] This concept was demonstrated through the artificially constructed composites, named the electromagnetic (EM) metamaterials.[2] The interest in these materials arises mainly from their anomalous physics not available in nature mediums, such as negative refraction, reversed Doppler shift, and reversed Cerenkov radiation.[3–5] These unusual effects promise a wide range of potential important applications such as superlens[4–6] and invisible cloak.[7,8] Recently, tremendous interest has also been extended to the acoustic analogue. Similarly to an EM wave transmitted in the EM metamaterials, acoustic wave propagating in the acoustic materials can be strongly modulated by using some special acoustic structures, leading to absolute band gaps in which waves could not propagate. The effective refractive index can be also modulated by the acoustic structure, and then a variety of applications, such as acoustic subwavelength imaging, may be produced.[9]

Up to now, the band gaps and strongly modified dispersions in the acoustic materials have been ascribed to two mechanisms. One is due to the Bragg scattering in composite materials with periodic variation of density and sound velocity. In particular frequency region where the wavelength is comparable with the periodic constant, the negative refraction can be induced due to the band-folding effect.[9–11] Negative refraction of acoustic wave, which can focus a diverging beam into a narrow focal spot, has been observed in a system consisting of periodic steel beads immersed in water.[9] Various periodic structures of this kind of acoustic materials have been widely studied both theoretically and experimentally.[9–11] The other is due to the local resonance. Local-resonant-type metamaterials have become of considerable interest in the EM metamaterials. Many representative models, such as split-ring resonator/thin wire (SRR/wire)[2,12] and periodically loaded transmission line (TL),[13–15] are proposed. However, few studies have been performed in the local-resonant-type acoustic materials.[16–19] Liu *et al.*[16] have demonstrated that some composites with locally resonant tuber-coated lead balls can exhibit effective negative elastic constants in certain frequency region. Most of other researchers adopted the similar model to Liu's.[17–19] Another type of local resonant acoustic materials is expected if the theory and concept for the EM metamaterials are extended to acoustics. Recently, Fang *et al.*[20] found a negative effective dynamic modulus near the resonant frequency in a structured composite which consists of a 1D array of repeated unit cells with shunted Helmholtz resonators (HR). The emergence of this composite has significantly broadened the range of the local-resonant-type acoustic materials. However, theoretical studies on this structure are only performed by Bloch wave theory and scattering theory based on perfect periodicity and infinite structure,[21,22] which have intrinsic limits such as their inflexibility to model complex quasiperiodic structure. In addition, as a consequence of the periodic arrangement of the resonators, the structure possesses the Bragg-type gap as well. Although the two types of bands originate from two different mechanisms, they may couple to each other if the periodic constant is small enough compared with the wavelength. This unique feature should be clarified further. On the other hand, it is intuitive to consider whether an ulterior step can be taken to derive a negative effective density as well even if a negative modulus has been reported by Fang *et al.*[20] The double-negativity (negative dynamic density and modulus) is indispensable to form a left-handed acoustic material, similarly to the negative permeability and permittivity in Veselago's medium.[1,23]

In this paper, we map the EM system into the acoustic analogues and extend the TL method used in EM analysis to the acoustic composites. With the acoustic transmission line method (ATLM), we derive the transmission coefficient and the phase velocity at various frequencies, and hence provide a simple physical picture of the one-dimensional (1D) acoustic structure. We employ coupled HRs and waveguides to produce anomalous response. We find that sound waves propagating in such a spatially periodic structure could be strongly modified and termed as "acoustic Bloch waves." In

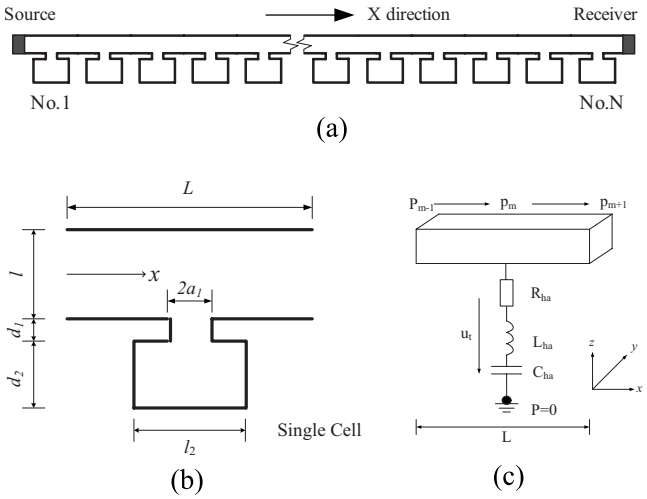

FIG. 1. (a) Schematic diagram of the 1D structured ultrasonic metamaterials consisting of unit cells with built-in Helmholtz resonators. (b) The cross-sectional picture and dimensions of a single cell. (c) The equivalent acoustic transmission line circuit of a unit cell, which consists of a waveguide section with distributed parameters and a parallel Helmholtz resonator with lumped parameters. *X* represents the direction of the sound wave propagation.

some frequency ranges, our materials exhibit some strong-coupled resonant states, which lead to the strong dispersive characteristics of the effective density and modulus simultaneously. These two constitutive parameters for acoustic materials exhibit a frequency region with simultaneously negative values. Thus such a system can behave as an effective left-handed medium for acoustic waves when the wavelength is much longer than the cell dimension. In particular, we have pay special attention to the influences of some essential configurations of geometric acoustic parameters on the transmission properties, such as periodic constant L. Numerical simulations by finite element method (FEM) are further carried out to demonstrate the ATLM results.

II. ATLM THEORY AND FORMULATIONS

Figure 1(a) shows the 1D structured ultrasonic metamaterials, which consist of a 1D array of repeated unit cells with shunted Helmholtz resonators. When the system is assembled, it behaves as a long two-end-open waveguide with small identical Helmholtz resonators (HRs) periodically loaded along one side.[20] The cross-sectional area of the HR's neck is small enough to assume that the resonators are connected at points along the waveguide. The unit cells are made up of metal and could be assumed as rigid walled. Sound wave propagates along the x direction and all field components are assumed to be independent of y and z direction.

When the wavelength is large enough compared with the transverse dimension of the duct, the sound wave transmitted in the interior of assembled waveguide is very nearly one-dimensional. We can assume it as plane wave if the frequency of the incident wave is under the cutoff frequency of the waveguide. In this long-wavelength approximation, the acoustic wave traveling in the waveguide is quite analogous to the electromagnetic wave propagating in the transmission line. The acoustic counterpart of voltage difference across an electric circuit part corresponds to the pressure difference across an acoustic element, while the current at points in the circuit is equivalent to the volume velocity of fluid in the corresponding acoustic element. In addition, HR can be considered as lumped circuit element in the shunt branch. Therefore, we can employ the well-known TL theory used for EM waves to study the acoustic materials.

A. Transmission coefficient

Before discussing the acoustic metamaterials, let us survey the EM counterpart. The common parameters used for characterizing the EM metamaterials are the electric permittivity $\varepsilon = n_{\mathrm{EM}}/Z_{\mathrm{EM}}$ and the magnetic permeability $\mu = n_{\mathrm{EM}} Z_{\mathrm{EM}}$,[24] where n_{EM} is the refractive index and Z_{EM} is the impedance for the EM medium. In TL theory, the EM wave propagation characteristics in materials and devices are characterized by three equivalent parameters: the inductance L_{EM}, the capacitance C_{EM} and the resistance R_{EM}.[24] In the present paper, we map these parameters into analogous acoustic system. Corresponding to ε and μ, we employ the density $\rho = n_{\mathrm{ac}} Z_{\mathrm{ac}}$ and the bulk modulus $\kappa = Z_{\mathrm{ac}}/n_{\mathrm{ac}}$ to specify the acoustic properties, where n_{ac} is the refractive index and Z_{ac} is the impedance for the acoustic medium, while the acoustic mass M_{ac}, capacitance C_{ac}, and resistance R_{ac} correspond to L_{EM}, C_{EM}, and R_{EM} in the EM metamaterials, respectively.[25,26] For plane waves incident on the metamaterials from water layer outside the metamaterials, the "refractive index" could be defined as the ratio of the wave vector in the metamaterials to that in water, i.e., $n_{\mathrm{ac}} = k_2/k_1$, or the ratio of the effective sound speed in water to that in the metamaterials, i.e., $n_{\mathrm{ac}} = c_1/c_2$. Here $c_1(c_2)$ and $k_1(k_2)$ are the effective sound speed and wave vector of water (metamaterials), respectively.

First, the acoustic property of the unit cell is investigated by means of ATLM.[26] In order to simplify the analysis, all cells used in the system have identical size, which should be considerably less than the wavelength, as shown in Fig. 1(a). Figure 1(b) shows a single cell, which is composed of a waveguide section and a shunt Helmholtz resonator consisting of a short neck and a cavity. X indicates the direction of the sound wave propagation. The cell is separated into two parts, i.e., a waveguide and a L-C circle, as shown in Fig. 1(c). The acoustic mass acting as inductor due to the short neck can be expressed as $M_{\mathrm{ha}} = \rho_w d_1/S_1$, and the cavity acts as a capacity with acoustic capacitance $C_{\mathrm{ha}} = S_2 d_2/\rho_w c_w^2$.[26] Here ρ_w is the density of fluid such as water, c_w is the sonic velocity in water, a_1 and d_1 are the radius and length of the short neck, l_2, w_2, and d_2 are the length, width, and depth of the cavity, and $S_1 = \pi a_1^2$ and $S_2 = l_2 \times w_2$ are the cross-sectional areas of the short neck and cavity, respectively, as shown in Fig. 1(b). On the other hand, the acoustic resistor R_{ha} consists of the viscosity $[R_{\mathrm{viscosity}} = (d_1/\pi a_1^3)\sqrt{2\eta\omega\rho_w}]$ and radiation $[R_{\mathrm{radiation}} = \rho_w c_w (ka_1)^2/S_1]$ parts, where ω is the angular frequency, k and η are the wave vector and coefficient of viscosity in water, respectively. The acoustic imped-

TABLE I. The material and structure parameters used in the calculation.

ρ_w (Kg/m^3)	c_w (m/s)	η'	d_1 (mm)	a_1 (mm)	d_2 (mm)	l_2 (mm)	w_2 (mm)	l (mm)
998	1483	1.85×10^{-5}	1	1	5	3.14	4	4

ance of a single Helmholtz resonator can be written as

$$Z_h = R_{\mathrm{ha}} + j\left(\omega M_{\mathrm{ha}} - \frac{1}{\omega C_{\mathrm{ha}}}\right). \tag{1}$$

When the HR is coupled to the waveguide, the consequent radiation effect of the opening should be included. Because of acoustic radiation, the short neck may become "longer." We call this equivalent extra mass radiation mass. So the effective length of short neck must be revised as $d_{\mathrm{effect}}=d_1+1.7a_1$,[26] and hence the resonant frequency can be expressed as

$$f_h = \frac{1}{2\pi\sqrt{M_{\mathrm{ha}}C_{\mathrm{ha}}}} = \frac{c_w}{2\pi\sqrt{\frac{S_2 d_2 d_{\mathrm{effect}}}{S_1}}}. \tag{2}$$

We assume the action of the fluid at the end of the waveguide as a piston which is open to free space.[26] This "virtual" piston radiates sound out into the surrounding medium, while a part of energy is reflected into the composite. In this case, the mechanical resistance ratio and reactance ratio are $r=(ka)^2/2$ and $x=8ka/3\pi$, respectively. The acoustic impedance induced by the mechanical radiation impedance through transformer is given by[26]

$$Z_{\mathrm{al}} = \frac{\rho_w c_w}{S_c} \times \left(\frac{k^2a^2}{2} + j\frac{8ka}{3\pi}\right), \tag{3}$$

where a is the effective radius of the piston and S_c is the cross-sectional area of the waveguide. Here, the acoustic resistance (real part) radiates the energy out and the acoustic reactance (imaginary part) reflects the energy back, similarly to that in the electromagnetic TL.[24]

Now, let us discuss the sound system with N cells, as shown in Fig. 1(a). It is well known that the terminal load can influence the incident wave. Based on the acoustic transmission line theory,[25,26] we employ an analysis method to analyze the transfer problem. The impedance of the end can be transferred to the position of the last HR neck using the acoustic transmission line impedance transfer formula[26]

$$Z'_{\mathrm{al}} = Z \times \frac{Z_{\mathrm{al}} + jZ\tan(KL)}{Z + jZ_{\mathrm{al}}\tan(KL)}. \tag{4}$$

Here, $Z=\rho_w c_w/S_c$ is the distributed impedance of the duct, and L is the distance between two adjacent HRs and could be assumed as a lattice constant. We also revise the wave number k as a complex one $K=k-j\alpha$, in order to include the absorption effects of the fluid. Here α is the absorption coefficient due to viscosity, which is proportional to the square of the frequency.

The transferred impedance Z'_{al} is parallel connected to the Nth resonator, and the parallel impedance is $Z_N=Z'_{\mathrm{al}}\|Z_h$. If Z_N is transferred to the $(N\text{-}1)$th HR's neck, which should be parallel connected to a shunt impedance Z_h, the acoustic impedance $Z'_N=Z\times\{[Z_N+jZ\tan(KL)]/[Z+jZ_N\tan(KL)]\}$ is obtained. By applying this process recursively for N times, we can transfer the lumped and distributed acoustic impedance of the whole system to the incident face of the composites. The iterative result Z_{eff} is the effective impedance of our composites with N cells. Thus, the sound pressure reflection coefficient r_p can be obtained from a simple formula $r_p=(Z_{\mathrm{eff}}-Z)/(Z_{\mathrm{eff}}+Z)$ if the sonic wave incidents normally along the duct, and the sound intensity reflection coefficient r_I and the intensity transmission coefficient T can be obtained to be $r_I=|r_p|^2$ and $T=1-r_I$, respectively. Note that the ATLM needs not invoke Bloch wave propagation or complex wave equations, and hence could be applied even in the random and quasiperiodic systems.

In order to demonstrate the band gap for the low frequency wave in the 1D periodic acoustic structure, we have calculated the transmission coefficient with finite units, i.e., $N=11$, 59, and 200. The acoustic properties of the fluid and the size of the cells utilized are listed in Table I. Here, all dimensions of the cavity should be considerably less than a wavelength, and the opening of the short neck should not be too large. We also configured the dimensions of the waveguide so as to make the cutoff frequency about 200 kHz. In order to compare our ATLM results with the published experimental data, we adopt some parameters reported by Fang *et al.*[20] Figure 2 shows the evolution of the transmission spectra for the composites with N cells: (a) $N=11$, (b) $N=59$, and (c) $N=200$. Here the periodic constant L is fixed to $\lambda/5$, where λ is the wavelength in the fluid at HR resonant frequency f_h (=32.1 kHz). We have found a significant band gap, in which the central frequency f_R is at 32.2 kHz and very close to f_h, as shown with a downward arrow in Fig. 2. Such a stop band has been ascribed to the absorption due to the local resonance of the HR cells. We also found some small adjacent bands outside 32.2 kHz, which are due to the coupled resonating between the HR cells. As the N-value increases from 11 to 200, the transmission spectrum becomes smooth. When $N=11$, it is also noted that a deep transmission band gap appears around 20 kHz, which is below the resonant band gap, as shown in Fig. 2(a). If increasing N to 59, the band gap becomes blurred, and then disappears when N reaches to 200 [see Figs. 2(b) and 2(c)]. The transmission band gap around 20 kHz may be ascribed to the undercoupling of the system due to insufficiency of the cells in the composite.[25,26] In fact, the wavelength at 20 kHz ($\approx$7.4 cm, 1.6λ) is comparable to the size of the structure with 11 cells ($\approx$10.1 cm, 2.2λ). Consequently, the transmission character is mostly affected by the waveguide, which has a low transmission coefficient around 20 kHz.[20,26] A Fano-like asymmetric transmission band has also been observed just below

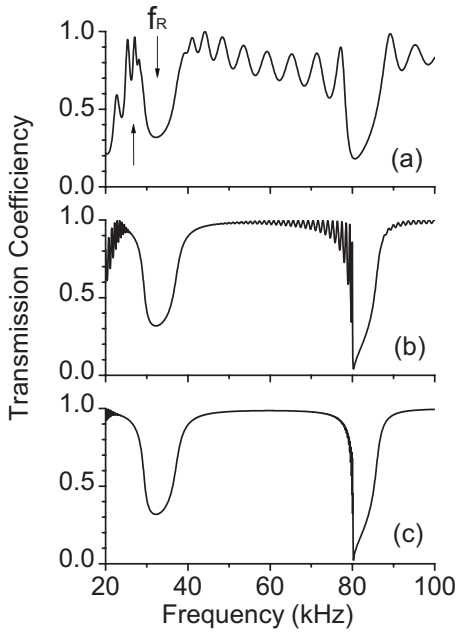

FIG. 2. Evolution of the transmission spectrum for metamaterials with (a) 11, (b) 59, and (c) 200 unit cells. The periodic constant L is fixed to $\lambda/5$. The upward and downward arrows in (a) indicate the Fano-like asymmetric transmission band and the center frequency f_R of local-resonant-type band gap, respectively. The band gap around 80 kHz is ascribed to the Bragg scattering effect.

the resonant band gap, as shown with an upward arrow in Fig. 2(a). This band should be ascribed to the nonresonant path in which part of the wave travels.[20] With further increasing the N value, the coupling is enhanced and the influence of the waveguide is weakened. As a consequence, the band around 20 kHz and the fluctuations in the transmission spectrum gradually disappear. It is also noted that there is another band gap appeared around 80.6 kHz, as shown in Fig. 2, which has been ascribed to the Bragg-scattering-type band gap. We also noted the difference of lowest transmission between this dip and the first dip around 32.2 kHz. This difference is attributed to their different originations. The first dip is local-resonant type, which is determined by the resonance of the HRs and could not be made quite low under practical conditions. In contrast, the second dip is Bragg-scattering type, which is determined by the intensive destructive interference by the periodic arrangement of the HRs in the propagation direction, having no relevancy with the resonance of HRs. Provided plenty of HRs and perfect periodicity, the lowest theoretical transmission could approach zero.

In order to understand the unique behavior observed above, the effective acoustic impedance of the composites Z_{eff} is discussed in detail in the system with 200 unit cells, as shown in Fig. 3. The real part of Z_{eff} (solid curve) and the image part (broken curve) are denoted as the acoustic resistance and the acoustic reactance, respectively. It is found that the resistance is quite small while the reactance is rather large in the frequency regions around 32.2 kHz and 80.6 kHz. We know that the resistance part produces the absorption of incident wave while the reactance part leads to the reflection of sound. Thus most of the incident energy in

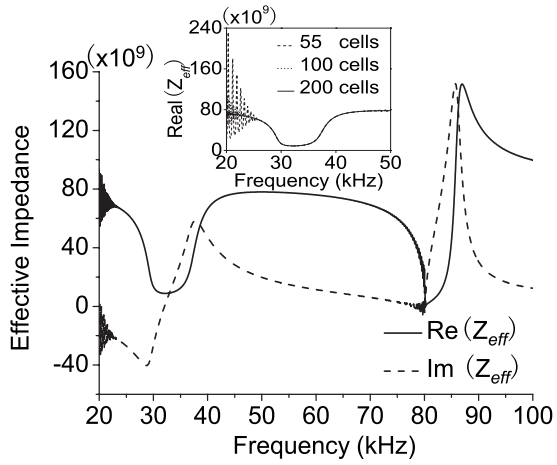

FIG. 3. Calculated dispersion curves of resistance (solid curve) and reactance (broken curve) for a sample with 200 cells. The inset shows the real parts of impedances with different unit cells. As the cell number increases, the impedance approaches an intrinsic value.

the regions at 32.2 kHz and 80.6 kHz is reflected back to the sound source and could not pass the composites. We should also emphasize that the low reactance and high resistance in the frequency regions outside the band gaps lead to the high transparency, i.e., the transmission coefficient approaches 1 for the wave in the pass bands, as shown in Fig. 2. In other words, our structure almost does not attenuate the acoustic energy outside the band gaps, except for little attenuation due to the fluid viscosity absorption. It is a significant advantage in practical applications such as high efficient frequency filters. The inset of Fig. 3 shows dispersion curves of the acoustic resistance with different cell numbers. It is found that the fluctuations appearing below 24 kHz disappear gradually as N increases from 59 to 200, which should be ascribed to the enhanced coupling mentioned above. The validity of assigning an effective impedance Z_{eff} to this structured noncontinuous material lies in the fact that Z_{eff} depends neither on the surface termination nor on the total length of the sample. So we can characterize the material by the intrinsic parameter Z_{eff}.

Let us continue to discuss the influence of geometric parameters on the transmission characteristic. Figures 4(a)–4(c) show the variation of the transmission coefficient with the different periodic constant L: (a) $L=\lambda/20$, (b) $L=\lambda/10$, and (c) $L=\lambda/5$. Here, the length of the composites is fixed to 1 m and the parameters of the single HR are set as same as that described in Table I. When $L=\lambda/20$, only local-resonant-type band gap appears, as shown in Fig. 4(a). With increasing L to $\lambda/10$, there is an extra band gap appearing at 160.4 kHz besides the local-resonant-type band gap [see Fig. 4(b)]. When $L=\lambda/5$, two new gaps appear at 80.2 kHz and 160.4 kHz, as shown in Fig. 4(c). We have further found that the positions of these extra band gaps are determined by an L value. The lowest frequency of these band gaps f_B obeys a simple relation $f_B=\lambda f_h/2\ L$, e.g., 80.2 kHz (160.4 kHz) at $L=\lambda/5$ ($L=\lambda/10$), as shown in Fig. 4(d). Other gaps appear at the integer multiple frequencies of f_B. These band gaps, induced by the periodic arrangement of the HRs, are ascribed

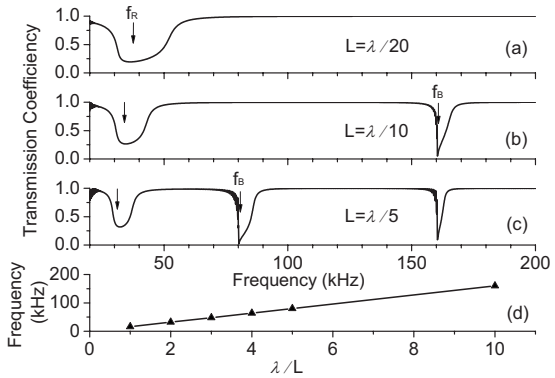

FIG. 4. Transmission coefficient for different periodic constants L: (a) $L=\lambda/20$, (b) $L=\lambda/10$, and (c) $L=\lambda/5$. The downward arrows indicate the center frequency f_R of the local-resonant-type band gap and the center frequency f_B of the lowest Bragg-scattering-type band gap, respectively. (d) λ/L dependence of the f_B values. The length of the composite is fixed to $1m$ and the parameters of single HR are the same as that listed in Table I.

to the Bragg-scattering effect. When the frequency of the incident wave equals to integer multiple of f_B, the phase accumulated in a cyclic through the periodic composites is an integer multiple of π. Consequently, the reflections due to the HRs are coherently enhanced, and hence the band gaps occur in the dispersion relation of the composites. These stop bands are referred to as the Bragg-scatting-type bands and emerge when the periodic constant becomes multiple of half-wavelength of the incident sound wave. In the view of effective impedance, this behavior is intelligible. When the frequency is close to the integer multiple of f_B, the $\tan(KL)$ term in Eq. (4) approaches zero, and hence the impedance transfer formula does not function. In this case, the system behaves as if the resonators are in parallel connection directly. Thus the parallel resistance part becomes very minute, while the reactance turns to quite large. As a result, the reflectivity of the wave becomes very large. In the other words, the band gaps are a consequence of the band-folding effect due to the periodic arrangement of the unit cells.

We also notice that the local resonant band becomes shallower and narrower with increasing L value. As shown in Fig. 4, the minimum transmission coefficient is 0.2 and the full width at half maximum (FWHM) for the absorption band is about 20.0 kHz when $L=\lambda/20$, while the respective results become 0.28 and 6.7 kHz when $L=\lambda/5$. Note that the periodic constant is several times smaller than the relevant wavelength in our composites. By combining the HRs into a periodic structure with so closed spatial lattice, there is strong acoustic coupling between the resonators. The larger the L value is, the weaker the coupling between the resonators becomes, and then the shallower and narrower the local resonant band changes. An obscure center frequency shift for the local resonant band gap is also observed with changing the L value, as shown by the downward arrows in Fig. 4. The center frequency f_R decreases from 36.3 kHz (34.5 kHz) at $L=\lambda/20$ ($L=\lambda/10$) to 32.2 kHz at $L=\lambda/5$, which has been ascribed to the weakened coupling between the adjacent HRs through the waveguide.

B. Phase velocity and group velocity

In order to characterize the acoustic wave propagation behavior in the metamaterials, the homogenized parameters should be extracted. The acoustic impedance per unit length due to the local resonant structure can be expressed as[26]

$$Z_w = (MS_1)^2 \times \left[\left(\frac{d_1\sqrt{2\eta\omega\rho_w}}{\pi a_1^3} + \frac{\rho_w c_w}{MS_1}\frac{(ka_1)^2}{2} \right) + j\omega\left(\frac{\rho_w d_{\text{effect}}}{MS_1} \right) - j\omega \Big/ \left(\frac{MS_2 d_2}{\rho_w c_w^2} \right) \right]. \quad (5)$$

Here $M=1/L$ is number of cells per unit length, and all other symbols are defined in above section.Z_w is capacitive in general. If considering the dissipation of the pipe wall, the coefficient of viscosity of the wall should be $l_v=\eta'/\rho_w c_w$, here η' is the coefficient of shear viscosity. Thus, the distributed acoustic resistance R_a, inductance L_a and capacitance C_a can be expressed as[26]

$$R_a = \rho_w c_w D k d_v / 2S_c^2, \quad (6)$$

$$L_a = \rho_w / S_c, \quad (7)$$

$$C_a = S_c/\rho_w c_w^2 + 1/j\omega Z_w. \quad (8)$$

Here, $d_v=\sqrt{2l_v c_w/\omega}$, and D is the cross-sectional perimeter of the square duct. In EM medium, a formula $K=\pm\sqrt{-ZY}$ is used to discuss the propagation constant.[24] In the acoustic material, the corresponding propagation constant such as $K=-j\sqrt{(R_a+j\omega L_a)(j\omega C_a)}$ can be obtained in the effective medium limit with $\lambda/L \gg 1$, which describes the phase relationship of acoustic wave in the effective medium. The dispersion relation reveals the variation of complex propagation constant with frequency. Figure 5 shows the dispersion relation for a representative acoustic metamaterial ($N=59$, $L=\lambda/5$) with frequency f: (a) real wave vector, (b) image wave vector and (c) the calculated group velocity, in which a significant jump occurs near 32.2 kHz. By comparing Fig. 2 with Fig. 5, we can obviously observe that there exists a frequency region in the local-resonant-type band gap in which the slope coefficient of the curve is negative. This result means the group velocity $v_g=(\partial k/\partial\omega)^{-1}$, which is the slope of the tangent to the f-k curve, is negative and in the opposite direction of phase velocity ω/k, as shown in Fig. 5(c). The origin of the negative group velocity will be discussed in the next section.

C. Double negativity

The simultaneous negativities for the effective permeability μ_{eff} and permittivity ε_{eff} can induce a negative refraction index for certain frequency ranges in the EM metamaterials with built-in local resonant structures.[3] In these composites, the EM wave equations assemble the 1D telegrapher's equations, which are expressed as[24]

$$-\frac{\partial H_z}{\partial x} = -j\omega\varepsilon_{\text{eff}} E_y, \quad (9)$$

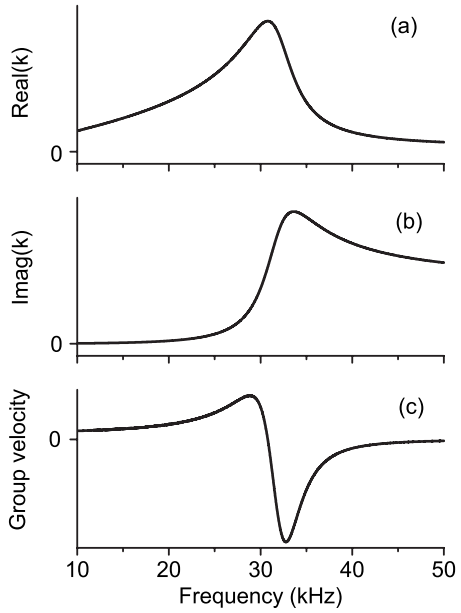

FIG. 5. Dispersion relation for a representative acoustic metamaterial ($N=59$, $L=\lambda/5$): (a) Real wave vector, (b) image wave vector, and (c) calculated group velocity. A significant jump occurs around 32.2 kHz, which indicates the negative group velocity.

$$-\frac{\partial E_y}{\partial x} = -j\omega\mu_{\text{eff}}H_z, \tag{10}$$

where H_z is the magnetic field in z direction, E_y is the electric field in y direction, and the EM waves travel along x direction.

In the acoustic materials, the 1D microscope acoustic wave equations in the lossless case can be expressed as[25,26]

$$-\frac{\partial p}{\partial x} = -j\omega\rho_{\text{eff}}u, \tag{11}$$

$$-\frac{\partial u}{\partial x} = -\frac{j\omega}{\kappa_{\text{eff}}}p, \tag{12}$$

where p is the sound pressure and u is the volume velocity. Here we neglect the harmonic dependence $e^{j\omega t}$. Comparing Eqs. (11) and (12) with Eqs. (9) and (10), the compressibility $1/\kappa_{\text{eff}}$, the density ρ_{eff}, and p and u correspond to the permeability μ_{eff}, the permittivity ε_{eff}, H_z, and E_y, respectively, in the EM metamaterials.

In order to characterize the acoustic metamaterials by constitutive parameters, we should derive the effective parameters κ_{eff} and ρ_{eff}. The propagation of the acoustic wave in mth unit can be described by approximate difference equations

$$-\frac{\partial p}{\partial x} = \frac{p_{m+1}-p_m}{L} = \frac{Z}{L}u, \tag{13}$$

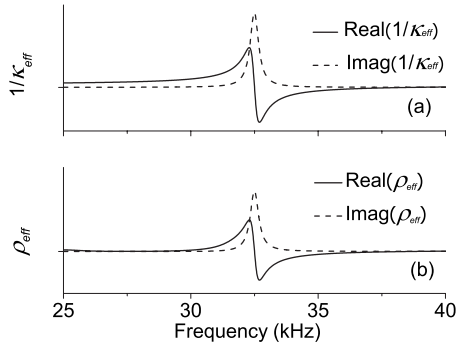

FIG. 6. (a) Effective bulk modulus and (b) dynamic density, in which the solid and broken curves stand for the real and image parts, respectively. Double negativity occurs in the frequency region around the center frequency f_R.

$$-\frac{\partial u}{\partial x} = \frac{u_{m+1}-u_m}{L} = \frac{Y}{L}p, \tag{14}$$

where $Y=1/Z_h$ is the admittance of a HR.

By combining Eqs. (11) and (12) and Eqs. (13) and (14), the effective bulk modulus of the structure in the lossless case can be obtained if we neglect the absorption due to viscous of the fluid,

$$\frac{1}{\kappa_{\text{eff}}} = \frac{1}{\kappa_0}\left(\frac{F\omega_0^2}{\omega_0^2-\omega^2}\right), \tag{15}$$

which is a function of frequency. Here, $\kappa_0(=\rho_w c_w^2)$ is the modulus of water and $F(=S_2d_2/S_cL)$ is the volume ratio of resonator cavity to waveguide section.

In EM metamaterials, the general form of permeability in the SRR/wire model is expressed as[2,3]

$$\mu_{\text{eff}}(\omega) = \mu_0\left(1-\frac{F\omega_0^2}{\omega^2-\omega_0^2+j\Gamma\omega}\right). \tag{16}$$

Thus the corresponding parameter such as the effective bulk modulus in the acoustic system can be expressed as

$$\frac{1}{\kappa_{\text{eff}}} = \frac{1}{\kappa_0}\left(1-\frac{F\omega_0^2}{\omega^2-\omega_0^2+j\Gamma\omega}\right). \tag{17}$$

Here, Γ is the intrinsic loss of the HR and could be obtained in the ultrasonic measurement. The equation shows that $1/\kappa_{\text{eff}}(\omega)$ acts like the permeability $\mu_{\text{eff}}(\omega)$ in SRR/wire model.[2,3] Figure 6(a) shows the calculated results for the dispersion of the effective modulus, in which the solid and broken curves stand for the real and image parts of the effective modulus, respectively. It is surprising that the real part of the $1/\kappa_{\text{eff}}(\omega)$ is negative in the resonant type band ($32.5\text{kHz}<f<37.0$ kHz).

It is well known that the refractive index n of a homogenous acoustic medium should be given by $n^2=\rho_{\text{eff}}\kappa_0/\rho_w\kappa_{\text{eff}}$. The negative κ_{eff} value means the possibility and necessity of the negative ρ_{eff}. Therefore, we need further procedure to extract ρ_{eff}. In the effective medium, the acoustic impedance of a material can be expressed as $Z_{\text{eff}}=\rho_{\text{eff}}c_{\text{eff}}$, where $c_{\text{eff}}(=\sqrt{\kappa_{\text{eff}}/\rho_{\text{eff}}})$ is the sonic speed in the

composites. Thus the ρ_{eff} value can be obtained from the Z_{eff} and κ_{eff} values. The dispersion of the ρ_{eff} value is shown in Fig. 6(b). The ρ_{eff} value is negative in the range of 32.5–38.7 kHz.

Generally, the effective mass density of structured material should be the volume-averaged mass density, which contains the implicit assumption of wave field homogeneity. This static density must equal to the ρ_w since only the vibration of the fluid functions in our metamaterials. Obviously we could not apply this static definition here. We should adopt the principle of dynamic mass density demonstrated by Mei *et al.*[27] The reason for the difference between the static and dynamic mass density may be ascribed to the fact that the field homogeneous assumption is violated. In order to testify our opinion, we further calculate the pressure filed intensities with FEM in the next section. The FEM calculated result indicates that the acoustic intensity within the resonators has a significant distinction with that in the waveguide [see Fig. 7(a)].

Comparing Fig. 6(a) with Fig. 6(b), it is noted that there is an overlapping region from 32.5 to 37.5 kHz, where both the effective density and bulk modulus have negative values. The negative frequency response means that the composites possess anomalous physical characteristics in the effective medium sense. Its deformation displacement and the load pressure should point to opposite directions. For example, it expands, not contracts, when compressed. Physically speaking, such a double negativity sounds impossible. So now the problem is why the effective parameters ρ_{eff} and κ_{eff} turn negative around f_R and how this process happens. In order to clarify the physics behind the double negativity, we return to our built-in local resonant structure. Obviously, every unit cell in our structure has a Helmholtz resonator. As described above, the HR is a harmonic oscillator in effect, which consists of a mass (fluid in the short neck) and a spring (fluid in the cavity). In the lossless case, the response of the oscillator to the exciting field is guided by $1/(\omega_0^2-\omega^2)$, and should be extremely large around ω_0. It is reasonable that the response function changes its phase by 180° and a large dispersion appears when ω exceeds ω_0. Since the resonator is connected to the waveguide, the oscillating field in the HR is coupled to the sound field in the waveguide. If we apply only one HR unit, the sonic wave is localized in the resonator and the coupled band gap is the origin of the double negativity. As we couple multiple HRs with the waveguide, these resonators can also be coupled together indirectly by the propagating wave in the waveguide besides the direct coupling between the neighboring HRs. Around the resonance frequency, the particle velocity in the necks becomes very large, as that in typical resonance. Meanwhile, the inertia of the fluid always accompanies with resonance. After several periodicities, all the HR units oscillate sufficiently and the acoustic field in the composites reaches steady state. The mass centers of the fluid in the necks vibrate in-phase strenuously. Thus the wave propagation is strongly modified by acoustic resonance induced by the resonators. If the frequency of the driven field exceeds ω_0, the oscillators in the unit cells could not change their phase immediately due to the inertia. In this case, the incident wave goes out of phase with respect to the motion of the fluid in the necks, and the fluid in the necks has enough momentum to resist the "push" of the acoustic field. Therefore the composites begin to retard the driven force and negative response appears.

Another important feature noted from Fig. 6 is that both the effective modulus and density take Lorentz form. This feature leads to a result distinguishing from SRR/wire system. In SRR/wire system, the transmission is low in double-negative frequency region ($\varepsilon_{\text{eff}}<0$, $\mu_{\text{eff}}<0$). However, the transmission is even lower in frequency range outside the double-negative region than that in the double-negative region. Thus the double-negative region of SRR/wire system behaves as a passband (see Ref. 2). In ultrasonic metamaterials, the transmission is also quite low in double-negative region ($\rho_{\text{eff}}<0$, $1/\kappa_{\text{eff}}<0$), like the situation in SRR/wire system. But contrastively, the transmission is higher in frequency range outside the double-negative region than that in the double-negative region. In this sense, the double-negative region of ultrasonic metamaterials behaves as a stop band.

In order to have further insight into the double negativity arising from resonance, we have compared the nature of acoustic metamaterial with its EM counterpart. Similarly to EM metamaterials, resonance is the key to archive negative response in artificial acoustic materials. In Liu's three-component sonic materials,[27] the local resonance is introduced artificially by unit cell consisting of a lead sphere core (acting as the mass) and a layer of silicone coat (acting as the spring). The acoustic properties of the component materials should contrast sharply. In our materials, the fluid in the short neck (acting as the mass) and the fluid in the cavity (acting as the spring) are employed to construct the local resonant unit. Both methods adopt the same principle of mass-spring system and produce similar negative response. Our system exhibits extra merit in that the fluid medium in the waveguide is also resonant synchronizing with the HR cells, which is a consequence of the identical component material we employed. This merit is an important origin of the double negativity.

In contrast, dissimilarly to EM metamaterials, the intrinsic origins of resonance of acoustic pressure p and volume velocity U in acoustic metamaterials are ambiguous. To understand how these quantities are produced, it is necessary to take the viewpoint of statistics. As we know, fluid is composed of millions of molecules. These molecules are in perpetual and random motion with various velocities and directions, which determine the gross properties of the fluid. If a sound probe is placed in the fluid, a lot of molecules bang against the sensor and a pressure is produced. (The volume velocity could also be understood in a similar way.) Applied disturbances, the adjacent medium are compressed and the statistical motion states of the molecules near the disturbance source are changed. As a consequence, p and U change. In inviscid fluid, large quantity of molecules will move back and forth in the direction of disturbance, producing adjacent regions of rarefaction and compression periodically. These disturbances can propagate through a compressible medium, and a wave is propagated. In conclusion, resonances of p and U in acoustic metamaterial are not introduced separately by separate structures as their EM counterparts E and H. They are produced simultaneously by the motion of the molecules and could not be obtained separately. This is an essential

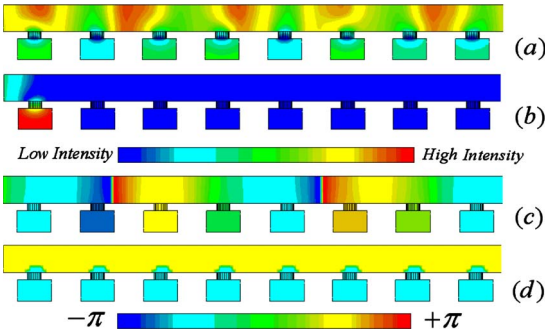

FIG. 7. (Color online) FEM simulations of the pressure field intensity at frequency (a) outside and (b) inside the local-resonant-type band gap and the phase distribution in the structure at frequency (c) below and (d) above the center frequency f_R. In (a) and (b), red and blue correspond to the high and low field intensities, respectively. In (c) and (d), red and blue indicate the phase with $+\pi$ and $-\pi$, respectively.

distinction between acoustic and EM metamaterials.

III. NUMERICAL SIMULATIONS BY FEM

The FEM is adopted to demonstrate the existence of resonant type band gaps in the structure and the validity of ATLM analysis due to its flexibility in modeling complex structures and its preponderance to get full field numerical solution.[28] In the FEM simulations, the wall of the duct and resonators is assumed to be rigid. Along the propagation direction (x direction), a monochromatic variation of displacements is imposed on the face of the inlet. Admittance derived from Eq. (3) is used to simulate the acoustic character of the open end. The whole structure is discretized into successive hexahedral elements. The six-elements-per-wavelength rule in acoustic mesh should be followed as a guideline.[28] It is also noted that the acoustic mesh should be reasonably regular, and the general accuracy is controlled by the largest elements in the mesh. The displacements interior to the elements, known as acoustic potential values and could be used to derive other acoustic parameters, are approximated in terms of their nodal values through the shape functions. The general FEM expression of Helmhlotz form wave equation can be written by[28]

$$([K] + i\omega[C] - \omega^2[M])\{p\} = \{F\}, \tag{18}$$

where the stiffness matrix $[K]$, damping matrix $[C]$, and mass matrix $[M]$, which are related with the properties of composites, are obtained by assembling elementary matrix through standard procedures. $\{F\}$ is the vector of nodal forces which is proportional to the normal velocity boundary conditions imposed on the faces of the model. The system of equations is set up to obtain the pressure distribution $\{p\}$.

Figure 7 shows the variation of the pressure field intensity calculated in frequency (a) outside and (b) inside the band gap. Color for red (blue) corresponds to the high (low) field intensity. The structure consists of 59 cells with $L=\lambda/5$. Other parameters are the same as that listed in Table I. As the frequency of incident wave is outside the band gap, the wave could be transmitted through the structure [Fig. 7(a)]. The distribution of the pressure field is periodic, which can be determined by the wavelength of the incident wave. Note that there is significant difference between the acoustic intensity within the cavity of HR and the waveguide. As a consequence, the pressure field is inhomogeneous and the condition of volume-averaged mass density is not satisfied.[27] In contrast with Fig. 7(a), the incident wave at the frequency in the gap could only penetrate the first few cells and the interior field is nearly zero, as shown in Fig. 7(b). The depth of penetration increases as the deviation from the center of the band gap f_R increases. In this case, the propagation of the wave is not permitted, and most of the incident energy is reflected backward. These results are consistent with those obtained by ATLM.

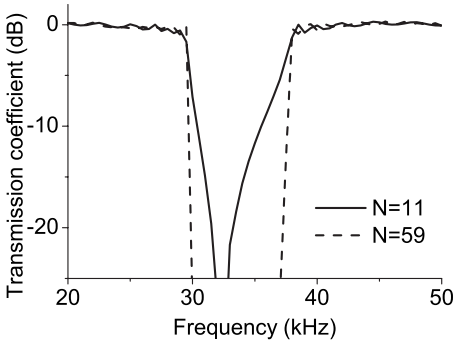

FIG. 8. The intensity transmission coefficient simulated by FEM with $N=11$ (solid curve) and $N=59$ (broken curve) unit cells.

Figures 7(c) and 7(d) show the phase distribution in the structure with various frequencies. Red and blue indicate phase with $+\pi$ and $-\pi$, respectively. The equiphase surfaces in the waveguide are parallel to each other, and perpendicular to the x direction, indicating that the acoustic wave propagating in the waveguide is a plane wave. The periodic variation of the phase distribution is determined by the wavelength of the incident wave. When $f<f_R$, the phase in the waveguide is the same as that in the resonator [see Fig. 7(c)]. In this case, the HR oscillates in-phase with the wave in the waveguide and the dynamic mass density must be positive. When $f>f_R$, the phase difference inside and outside the resonator in each cell is always π [see Fig. 7(d)]. In this case, the HR oscillates out of phase with the wave in the waveguide, and the dynamic mass density could turn negative if the oscillation is strong enough.

With the obtained $\{p\}$, we further calculate the transmission spectrum of the system with finite units. Figure 8 shows the intensity transmission coefficient as a function of frequency for 1D composites with 11 (solid curve) and 59 (broken curve) unit cells. Here, the material and geometric parameters are same as that listed in Table I, and the periodic constant L is adopted as $\lambda/5$. In the composites with 11 cells, a narrow and shallow gap appears in the transmission spectrum in the frequency region from 29.5 to 38.0 kHz, as shown by the solid curve in Fig. 8. With the increase of the unit cells to 59, the gap becomes wider and deeper, as shown by the broken curve in Fig. 8. In addition, the band edge with 59 cells is much steeper than that with 11 cells. As more cells

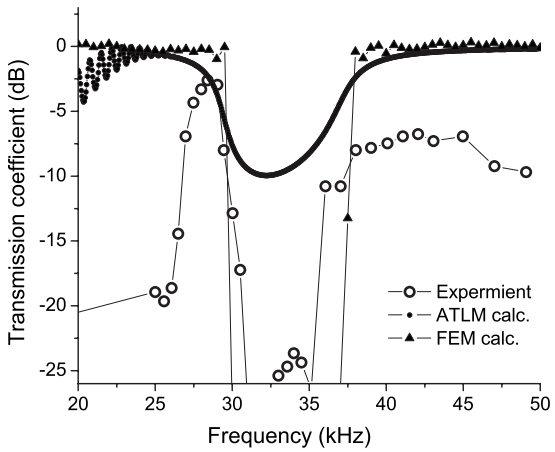

FIG. 9. Frequency dependence of the transmission coefficient: The curves with the open circles, solid circles, and solid triangles represent the experimental data (cited from Ref. 20), ATLM, and FEM simulation results, respectively.

are employed, the resonance absorber effect is enhanced significantly (not shown). The FEM results are similar to that with ATLM (see Fig. 2).

Finally, let us compare the FEM and ATLM simulated results ($N=59$, $L=\lambda/5$) with the experimental data reported by Fang *et al.*[20] Figure 9 shows frequency dependence of the transmission coefficient: The curves with open circles, solid circles, and solid triangles represent the experimental data, ATLM, and FEM simulation results, respectively. It is found that the forbidden band locates around f_R ($\sim$32.2 kHz) for all situations. It is noted that there are differences in lowest transmission between the ATLM results, the experiments and the FEM results. These differences are attributed to the inherent limitations of ATLM, experiments and FEM. ATLM characterizes the acoustic feature of metamaterial with complex geometry by simplified effective parameters. In these parameters, the viscosity coefficient employed here only describes the acoustic absorption in fluids and could not model the wall effect in pipes. The experiment is determined by the sensitivity of the hydrophones and could not measure data below noise floor of the equipment. In FEM, the system is modeled using fluid with parameters determined empirically, which may be different from practical situation.[26]

IV. CONCLUSION

We have proposed an acoustic transmission line equivalent circuit model to analyze the ultrasonic wave propagation in the 1D ultrasonic metamaterials with periodically loaded built-in Helmholtz resonators. We have examined the transmission coefficient, propagation constant, effective density, and bulk modulus based on the acoustic transmission line method. Field intensity, phase distribution, and transmission coefficient for finite unit system is also obtained through FEM simulations to reconfirm the ATLM results. Essential configurations of geometric acoustic parameters, such as periodic constant L, are also systematically discussed. It should be emphasized that the double negativity results from local resonance and is not a consequence of the traditional Bragg scatting. So the size of the cell no longer depends on the wavelength of the related sound wave. Evidently, this kind of composites offer great flexibility in tailing the position of band gap by varying the size of loaded resonators. Furthermore, the bandwidth may be made arbitrarily large by periodically loading appropriately designed Helmholtz resonators with different parameters. In that condition, due to the periodicity, the single resonant frequency will extend to a wide stop band. Such flexibility means that it is quite easy to fabricate and test this type of metamaterial as we need. In addition, a more detailed study is in progress to clarify the anomalous double negativity in the two- and three-dimensional systems.

ACKNOWLEDGMENTS

This work was supported by the National Natural Science Foundation of China under Grant No. 10574071 and 10374041, the Key Project of Chinese Ministry of Education under Grant No. 107051, and the program for New Century Excellent Talents in Chinese University under Grant No. NECT-04-0456.

*Corresponding author. Address: Key Lab of Modern Acoustics, Nanjing University, Nanjing 210093, China. FAX: +86-25-83315557. liuxiaojun@nju.edu.cn

[1] V. G. Veselago, Sov. Phys. Usp. **10**, 509 (1968).
[2] D. R. Smith, W. J. Padilla, D. C. Vier, S. C. Nemat-Nasser, and S. Schultz, Phys. Rev. Lett. **84**, 4184 (2000).
[3] R. A. Shelby, D. R. Smith, and S. Schultz, Science **292**, 77 (2001).
[4] D. R. Smith and N. Kroll, Phys. Rev. Lett. **85**, 2933 (2000).
[5] A. K. Iyer, P. C. Kremer, and G. V. Eleftheriades, Opt. Express **11**, 696 (2003).
[6] A. Grbic and G. V. Eleftheriades, Phys. Rev. Lett. **92**, 117403 (2004).
[7] J. B. Pentry, D. Schurig, and D. R. Smith, Science **312**, 1780 (2006).
[8] D. Schurig, J. J. Mock, B. J. Justice, S. A. Cummer, J. B. Pendry, A. F. Starr, and D. R. Smith, Science **314**, 977 (2006).
[9] S. X. Yang, J. H. Page, Z. Y. Liu, M. L. Cowan, C. T. Chan, and P. Sheng, Phys. Rev. Lett. **93**, 024301 (2004).
[10] X. H. Hu, Y. F. Shen, X. H. Liu, R. T. Fu, and J. Zi, Phys. Rev. E **69**, 030201(R) (2004).
[11] S. X. Yang, J. H. Page, Z. Y. Liu, M. L. Cowan, C. T. Chan, and P. Sheng, Phys. Rev. Lett. **88**, 104301 (2002).
[12] D. R. Smith and D. Schurig, Phys. Rev. Lett. **90**, 077405 (2003).
[13] G. V. Eleftheriades, O. Siddiqui, and A. K. Iyer, IEEE Microw. Wirel. Compon. Lett. **13** (2), 51 (2003).
[14] Y. J. Feng, X. H. Teng, Y. Chen, and T. Jiang, Phys. Rev. B **72**, 245107 (2005).

[15] G. V. Eleftheriades and K. G. Balmain, *Negative-Refraction Metamaterials* 1st ed. (Wiley, New York, 2005).
[16] Z. Y. Liu, X. X. Zhang, Y. W. Mao, Y. Y. Zhu, Z. Y. Yang, C. T. Chan, and P. Sheng, Science **289**, 1734 (2000).
[17] C. Goffaux, J. Sanchez-Dehesa, A. L. Yeyati, Ph. Lambin, A. Khelif, J. O. Vasseur, and B. Djafari-Rouhani, Phys. Rev. Lett. **88**, 225502 (2002).
[18] R. Sainidou, B. Djafari-Rouhani, Y. Pennec, and J. O. Vasseur, Phys. Rev. B **73**, 024302 (2006).
[19] G. Wang, X. S. Wen, J. H. Wen, L. H. Shao, and Y. Z. Liu, Phys. Rev. Lett. **93**, 154302 (2004).
[20] N. Fang, D. J. Xi, J. Y. Xu, M. Ambati, W. Srituravanich, C. Sun, and X. Zhang, Nat. Mater. **5**, 452 (2006).
[21] C. E. Bradley, J. Acoust. Soc. Am. **96**, 1844 (1994).
[22] N. Sugimoto and T. Horioka, J. Acoust. Soc. Am. **97**, 1446 (1995).
[23] J. S. Li and C. T. Chan, Phys. Rev. E **70**, 055602(R) (2004).
[24] J. A. Kong, *Electromagnetic Wave Theory* (Wiley, New York, 1986).
[25] K. U. Ingard and P. M. Morse, *Theoretical Acoustic* (McGraw-Hill, New York, 1968).
[26] L. E. Kinsler, *Fundamentals of Acoustic*, 3rd ed. (Wiley, New York, 1982).
[27] J. Mei, Z. Y. Liu, W. J. Wen, and P. Sheng, Phys. Rev. Lett. **96**, 024301 (2006).
[28] O. Z. Zienkiewicz and R. L. Taylor, *The Finite Element Method*, 5th ed. (Elsevier, Singapore, 2004).